

The effect of the magnetically dead layer on the magnetization and the magnetic anisotropy of the dextran-coated magnetite nanoparticles

Zhila Shaterabadi^{1,2} · Gholamreza Nabiyouni^{1,2} · Gerardo F Goya³ · Meysam Soleymani⁴

1. Department of Physics, Faculty of Science, Arak University, Arak, 38156-88349, Iran
2. Department of Chemical Engineering, Faculty of Engineering, Arak University, Arak, 38156-88349, Iran
3. Condensed Matter Physics Department, Faculty of Sciences & Institute of Nanoscience and Materials of Aragón, University of Zaragoza, Zaragoza, Spain.
4. Institute of Nanoscience and Nanotechnology, Arak university, Arak, Iran

Abstract

We present a study on the magnetic behavior of dextran-coated Fe₃O₄ magnetic nanoparticles (Dex-M NPs) with sizes between 3 and 19 nm, synthesized by hydrothermal-assisted co-precipitation method. The decrease of saturation magnetization M_s with decreasing particle size has been modeled by assuming the existence of a spin-disordered layer at the particle surface, which is magnetically dead. Based on this core-shell model, the dead layer thickness (t) and saturation magnetization (M_s) of the magnetic cores in our samples were estimated to be $t = 6.8 \text{ \AA}$ and $M_s = 98.8 \text{ emu/g}$, respectively. The data of M_s was analysed using a law of approach to saturation, indicating an increase in effective magnetic anisotropy (K_{eff}) with decreasing the particle size as expected from the increased surface/volume ratio in small MNPs. The obtained K_{eff} were successfully modeled by including an extra contribution from dipolar interactions due to the formation of chain-like structure of MNPs. The surface magnetic anisotropy (K_s) was estimated to be about $K_s = 1.04 \times 10^5 \text{ J/m}^3$. Our method provides a simple and accurate way to obtain the M_s core values in surface-disordered MNPs, a relevant parameter required for magnetic modeling in many applications.

Keywords: Magnetic dead layer, Core-shell model, Spin disorder, Surface magnetic anisotropy, Dextran-coated magnetite NPs.

1. Introduction

Particle size reduction to the nanometer scale significantly affects magnetic properties of magnetic nanoparticles (MNPs) due to deleterious impact of surface atoms on the effective magnetization of the MNPs [1, 2]. However, when optimal performance is seek in bio-applications such as magnetic hyperthermia therapy [3, 4], drug delivery [5, 6], and magnetic resonance imaging [7, 8], it is important to retain the magnetization values M at room temperature as close as possible to the corresponding bulk ones [9, 10]. Hence, it is important to address size-dependent changes of magnetic properties in nanometer-scaled particles.

As the size of the MNPs decreases below the micrometer-size range several new phenomena appear, including superparamagnetism [11, 12], reduced saturation magnetization [13, 14], non-saturated and open hysteresis loop at high magnetic fields [15, 16]. For a given material with effective magnetic anisotropy K_{eff} , the superparamagnetic behavior appears when the particle volume V is small enough that the thermal energy can overcome the anisotropy energy barrier $E = K_{\text{eff}} V$ separating magnetization easy axes [17, 18]. On the other hand, the reduced and non-saturating magnetization phenomena originate from spin-disordered configuration at the MNP surface, that can be explained by the core-shell model.

This core-shell configuration on MNPs consists of a spin-disordered shell, known as magnetic dead layer (due to its zero net magnetization), surrounding a core with ferro/ferri magnetic-ordered spins [19, 20]. Deterioration of magnetic order in the dead layer is originated from the surface effects in this region. In fact, structural distortions at the MNPs boundaries result in breaking atomic bonds and consequently frustrating exchange interactions between surface and core spins, which in turn lead to the orientation deviation of surface spins with respect to the core ones [19, 21-24]. In ferrites, like magnetite, exchange interactions occur through intermediation of oxygen

ions (called super-exchange interactions), and therefore the presence of defects and impurities in surface sites or missing of oxygen ions can spread the spin-disordered region into the core [21-23].

Consequently, the decrease in M_s with the size reduction, which is one consequence of surface effects, has been well described by considering a model in which the MNPs are composed with a core having bulk-like magnetic properties and a surrounding shell composed of a magnetically disordered layer. In fact, as the particle size decreases the impaired magnetic order of the surface layer increasingly determines the magnetic properties of a given MNP. For iron oxide NPs with 0.9 nm magnetic dead layer thickness, Kim et al. reported that 61.4% of spins in 12 nm-sized MNPs are magnetically disordered, while the figure increasingly reaches 99.4% in 2.2 nm-sized MNPs [25]. In addition, the decreasing trend of M_s with the size reduction has been reported in many articles [26-33]. Nevertheless, to the best of our knowledge, only one experimentally-estimated value has ever been reported for the magnetic dead layer thickness of magnetite NPs, not considering the coating ligand-related effect on the measured magnetization [34].

In this work, variable-sized Dex-M-NPs (from 3.1 to 18.9 nm) synthesized for magnetic hyperthermia [35] were used to investigate the effect of size reduction on the magnetization behavior. Specifically, we estimated the magnetic dead layer thickness of Dex-M NPs using real values of M_s at high magnetic fields for the magnetic part of Dex-M NPs by eliminating the weight contribution of non-magnetic coating layer to the whole magnetization. The obtained results can provide new insight into the modification of magnetic properties of MNPs, especially for applications in which an accurate determination of M_s is required, for instance magnetic heating models, magnetic actuation, etc.

2. Results and discussion

The Dex-M NPs in the size range 3.1–18.9 nm were synthesized by combination of co-precipitation and hydrothermal methods. The details of experimental procedure and sample characterization are given elsewhere [35]. The synthesis conditions of samples as well as some samples characteristics (e.g. M_s , TEM particle size (D), and the percentage of remanence mass in TG analyses (m_r)) are summarized in Table 1. We note that our largest applied field in VSM measurements could be insufficient for complete saturation of samples, and thus the M_s^* values were estimated using extrapolation of magnetization (M) versus the inverse of magnetic field strength ($1/H$) curves. To this end, initial magnetization curves of Dex-M-NPs (shown in Fig. 1) were utilized to make M vs. $\frac{1}{H}$ curves using their data near saturation. Both the M_s^* and M_s values are presented per unit of total mass ($g_{\text{Dex-M}}$) which comprises the mass of magnetite NPs (g_{Mag}), dextran layer, and absorbed water on NPs surface. Therefore, M_s^{**} values (real saturation magnetizations at high magnetic field strengths for pure magnetite NPs) were estimated using effective magnetic material mass obtained by m_r in TG analyses. The values of M_s^* , and M_s^{**} are also summarized in the Table 1.

Table 1 Synthesis conditions, TEM particle size, and some characteristics of the Dex-M NPs

Sample	Synthesis conditions*	D (nm)	M_s (emu/ $g_{\text{Dex-M}}$)	m_r (%)	M_s^* (emu/ $g_{\text{Dex-M}}$)	M_s^{**} (emu/ g_{Mag})
Dex-M-80	Co 80°C	3.1±0.4	8.3	60.73	9.9	16.3
Dex-M-120	Co80°C+Hy120°C	4.5±0.4	26.5	72.66	27.9	38.4
Dex-M-140	Co80°C+Hy140°C	6.7±0.3	33.8	80.60	34.9	43.3
Dex-M-160	Co80°C+Hy160°C	8.1±0.2	44.4	82.21	45.3	55.1
Dex-M-180	Co80°C+Hy180°C	11.5±0.2	59.2	82.62	59.9	72.5
Dex-M-200	Co80°C+Hy200°C	15.0±0.3	64	86.38	64.7	74.9
Dex-M-220	Co80°C+Hy220°C	18.9±0.3	67.9	87.69	68.4	78

* Co-precipitation and hydrothermal synthesis methods are respectively written as Co and Hy for short. Also, the synthesis temperature is written next to each method name.

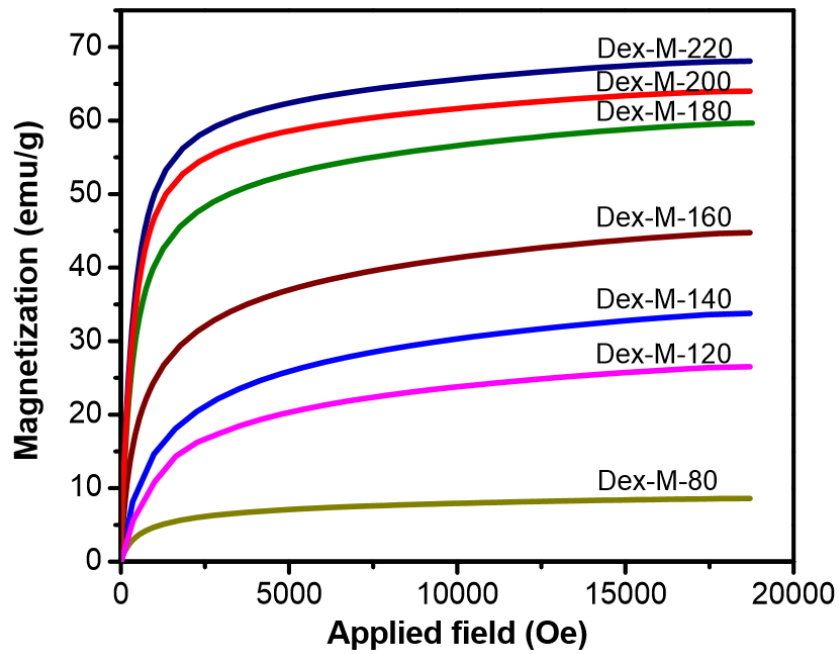


Fig. 1 Initial magnetization curves of Dex-M-NPs as a function of applied magnetic field

As it can be seen in the Table 1, M_s^{**} values are smaller than those of the bulk material in the range 84 – 100 emu/g [17, 33, 36-38]. Moreover, they dramatically decrease with the particle size reduction. Decline in the saturation magnetization with decrease in the particle size, which has already been observed in other experimental works [39-43], can be originated both from redistribution of cations between two sub-lattices of spinel structure and spin disorder on the particle surface. It has been reported that the distribution of cations between tetrahedral and octahedral sites of spinel structure can significantly affect the magnetization of ferrite NPs [76]. Magnetite (Fe_3O_4) is an interesting member of the spinel ferrite family with inverse structure as $(Fe^{3+})(Fe^{2+}Fe^{3+})O_4$ in which the parentheses respectively indicate the tetrahedral and octahedral sites [4,76]. Consideration the magnetic moments of Fe^{3+} and Fe^{2+} ions as 5 and 4 μ_B respectively, the net magnetic moment of each magnetite molecule is simply calculated as 4 μ_B . Assuming the probable redistribution of a fraction (x) of cations, a partially deviated inverse spinel structure as $(Fe^{2+}_x Fe^{3+}_{1-x})(Fe^{2+}_{1-x} Fe^{3+}_{1+x})O_4$ with the net magnetic moment $(4 + 2x) \mu_B$ is formed [44].

Accordingly, even if the size reduction causes a change in the arrangement of cations in the spinel structure of the magnetite NPs, magnetization is expected to increase. In other words, the magnetization reduction can exclusively be attributed to the existence of the magnetically inert layer on the surface of the MNPs in the core-shell model.

Assuming that the magnetic dead layer has a) a negligible net magnetization and b) a thickness, t , independent of particle size, D , the saturation magnetization M_s is given by

$$M_s = M_{s0} (1 - 2t/D)^3 \quad (1)$$

where M_{s0} is the saturation magnetization of bulk material. Ec.(1) indicates that the decrease of our experimental values of M_s^{**} (i.e., the magnetization corrected for the dextran mass) should be most relevant for the smallest MNPs. The plot of $M_s^{**1/3}$ vs. $1/D$ data (Fig. 2) could be well fitted by a linear function as expected from Ec. (1), obtaining the values of $M_{s0} = 98.8$ emu/g and $t = 6.8$ Å for the bulk saturation magnetization and dead layer thickness, respectively ($R^2 = 0.9662$).

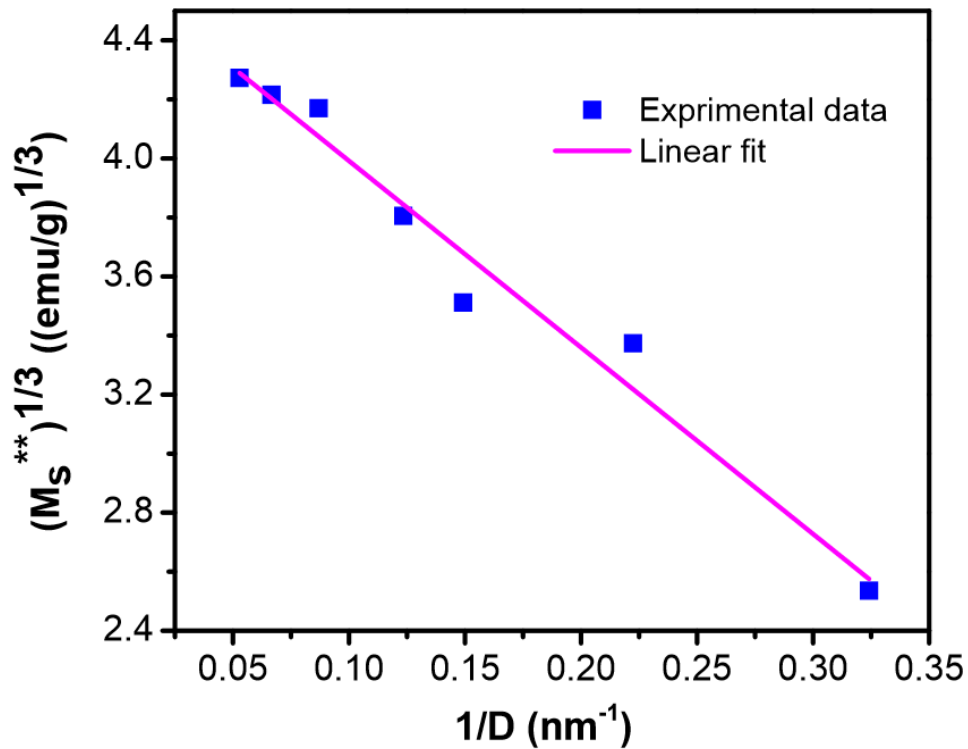


Fig. 2 The cube root of saturation magnetization ($M_s^{**1/3}$) versus the inverse of average diameter ($1/D$) of Dex-M-NPs

The M_{s0} obtained from the fit is consistent with reported values of bulk magnetite (95.0-98.5 emu/g) [17, 33, 36-38]. The value of the thickness $t = 6.8 \text{ \AA}$ obtained from the fit is somewhat smaller than the Fe_3O_4 lattice constant (8.39 \AA) [45] but comparable to previous findings $t = 6 \text{ \AA}$ found by Chen et al. [46], and Zheng et al. [47] for MnFe_2O_4 NPs at 300 K. Other t values consistent with our findings have been reported in different systems, including values of $t = 5 \text{ \AA}$ (at 10 K) [46], and 4.5 \AA (at 20 K) [48] for MnFe_2O_4 MNPs, and 10 \AA (at 5 K) for CoFe_2O_4 NPs [49]. Interestingly, CuFe_2O_4 NPs with sizes from 10 to 60 nm produced by mechanical milling were reported to have a much larger $t \approx 2.5 \text{ nm}$ spin-disordered layer thickness, consistent with the high-energy collisions during mechanosynthesis [50]. The only measured values for the thickness t in Fe_3O_4 MNPs, to the best of our knowledge, has been reported by Caruntu et al. to be $t = 2.26 \text{ \AA}$ (at 300 K) and $t = 1.92 \text{ \AA}$ (at 5 K) [34]. Although these values are smaller than the estimation presented here, comparison between samples obtained from different synthesis routes can be misleading, since the thickness of the disordered surface is expected to depend on the details of the energy landscape involved in each synthesis route. We also note that the thickness t obtained from the extrapolation method could be affected by the M_s values assumed for the magnetic core at high magnetic field. Our estimations are based on considering the M_s^{**} value obtained from the extrapolation of M vs. $1/H$ curves and the TG results.

Using the obtained t value and assuming the spherical shape for the Dex-M NPs, the magnetic-disordered content for the Dex-M-80 NPs was calculated to be 82.3 %. It means that the magnetic order only exists in 17.7% of the particle volume. By increasing the particle size, the magnetic-ordered content increases to 79.9 % for the Dex-M-220 NPs. Therefore, the effect of surface

magnetic disorder on the magnetic behavior of MNPs significantly diminishes with increasing the particle size, consistent with the decrease of the surface/volume ratio as the particle size increases.

The magnetization data as a function of the applied field H can be analyzed in terms of the law of approach to saturation [51]:

$$M = M_S \left(1 - \frac{b}{H^2} \right) \quad (2)$$

where the parameter b is related to the magnetocrystalline anisotropy, which can be obtained from the $M(H)$ data near saturation by a linear fitting of the $\frac{M}{M_S}$ (or $\frac{M^{**}}{M_S^{**}}$ in our assumption) versus $1/H^2$ curve. Following the procedure reported in [52], we calculated K_{eff} for a uniaxial magnetic anisotropy as Eq. (3) [53, 54].

$$K_{\text{eff}} = \mu_0 M_S \left(\frac{15}{4} b \right)^{1/2} \quad (3)$$

Using the b values obtained from Eq. (2) and the M_S^{**} values from Table 1, Eq. (3) yielded the K_{eff} values for Dex-M NPs listed in Table 2. These calculated values are higher than the bulk anisotropy constant ($K_{\text{bulk magnetite}} = 1.35 \times 10^4 \text{ J/m}^3$ [55]), reflecting the surface effects as particle size decreases. This size dependence is consistent with previous findings in iron oxide NPs [34, 52, 55, 56] that reported a rising trend for K_{eff} with size reduction. The size dependency of the K_{eff} is in good agreement with previous results on spherical Fe_3O_4 MNPs showing a decrease in K_{eff} from $4.74 \times 10^5 \text{ J/m}^3$ to $1.11 \times 10^5 \text{ J/m}^3$ with increasing particle size from 6 to 11 nm [34]. Similar changes in the K_{eff} for cubic magnetite NPs have been observed, with a reduction from $77 \times 10^3 \text{ J/m}^3$ (20 nm diameter) to $42 \times 10^3 \text{ J/m}^3$ (40 nm diameter) [52]. Sarkar and Mandal also reported a decreasing trend in the K_{eff} from $1.84 \times 10^5 \text{ J/m}^3$ (7.23 nm diameter) to $1.25 \times 10^5 \text{ J/m}^3$ (11 nm diameter) for chain-like magnetite NPs [55].

We mention that, since the overall shape of our MNPs does not change significantly along the series of samples as observed from TEM images,[35] the contributions from shape anisotropy to K_{eff} can be ignored.

Assuming that the magnetocrystalline anisotropy K_{bulk} of the magnetic cores is constant along our series of samples with different particle sizes, additional contributions to the *effective* magnetic anisotropy K_{eff} come from shape and/or surface as well as magnetic dipolar interactions among MNPs [57-59]. Our experimental determination of the evolution in both K_{eff} and K_S was made on non-diluted samples, so dipolar magnetic interparticle interactions could be not negligible in the analysis of the single-particle magnetic anisotropy. However, the dextran-coating makes the MNPs to be separated by (at least) a distance twice the coating layer thickness, and therefore dipole-dipole interactions between particles can be assumed to be constant along our sample series [34, 60, 61]. Additionally, since the M_s values in our MNPs decrease with decreasing particle size (see Table 1) the same trend are to be expected for the strength of dipole-dipole interactions [61].

The phenomenological expression for the anisotropy K_{eff} originally proposed by Bødker et al. [62],

$$K_{\text{eff}}V \cong K_{\text{bulk}}V + K_S S \quad (4)$$

where K_{bulk} is the bulk anisotropy energy per unit volume, and K_S is the surface density of anisotropy energy. Assuming that the particles are spherical with diameter D , Bødker et al. simplified the Eq. (4) as Eq. (5) which has been experimentally found on many different systems [63, 64].

$$K_{\text{eff}} \cong K_{\text{bulk}} + \frac{6K_S}{\langle D \rangle} \quad (5)$$

Using symmetry arguments and assuming that surface anisotropy is normal to the particle surface, Bødker et al. [62] showed that for a perfectly spherical particle a zero contribution from surface anisotropy should be expected. We note here that this is an empirical expression, and the

hypothesis that the surface contribution to the effective anisotropy is simply additive has yet to be demonstrated.

Fig. 3(a) shows fitting the K_{eff} vs. $1/D$ data using Eq. (5), from which a value $K_s = 2.11 \times 10^5 \text{ J/m}^3$ was obtained for our Dex-M NPs samples. However, as clearly seen in Fig. 3(a), there is a large deviation from the linear behaviour for large $1/D$ values. These deviations could be explained by deviations from spherical shape that are not included in Eq. (5). Indeed, for different particle morphologies Eq. (4) should include an additional contribution with a different K_{eff} vs. $\frac{1}{D}$ slope. However, as previously mentioned no major change in MNPs morphology can be observed in our series of increasing-size samples, in spite of the hydrothermal route used.[35, 65-67].

It should be noted that in the original work by Bødker et al., did not consider any contributions from dipolar interactions to the collective behavior of nanoparticles. It is well known that dipolar interactions between MNPs favor the formation of the chain-like structure in large enough MNPs for which the energy of the magnetic dipole-dipole interaction energy can surpass the thermal energy even at room temperature [68-73]. To include these interactions, we modified Eqs. 4 and 5 including a parabolic term

$$K_{\text{eff}} \cong K_{\text{bulk}} + \frac{6K_s}{\langle D \rangle} + \frac{E_1}{\langle D^2 \rangle} \quad (6)$$

in which E_1 has units of a linear density of anisotropy energy. Fig. 3(b) clearly shows that using Eq. (6) the fit of experimental data can be extended to the full range of particle sizes. The last term in Ec. (6) could be understood as originated in the formation of one-dimensional chains of MNPs (i.e. head-to-tail orientation) due to dipolar interactions. Consistent with Ec.(6) the last term is more relevant for larger $1/D$ values, reflecting the fact that chain formation is favoured for larger MNPs due to their larger dipolar moment. This interaction originates the extra contribution to the

anisotropy in the Eq. (6) and, with this assumption and using Eq. (6) to fit the K_{eff} vs. $1/D$ data, a value of $K_s = 1.04 \times 10^5 \text{ J/m}^3$ was obtained for our Dex-M NPs samples. The obtained value shows that surface anisotropy gives an important contribution to the effective anisotropy of small MNPs. In fact, surface anisotropy originates from the lack of long-range crystalline order in surface layer where breaking the crystal structure symmetry due to the lower and more variable coordination of cations results in perturbation in crystal field and consequently modification of magnetocrystalline anisotropy. [21, 23].

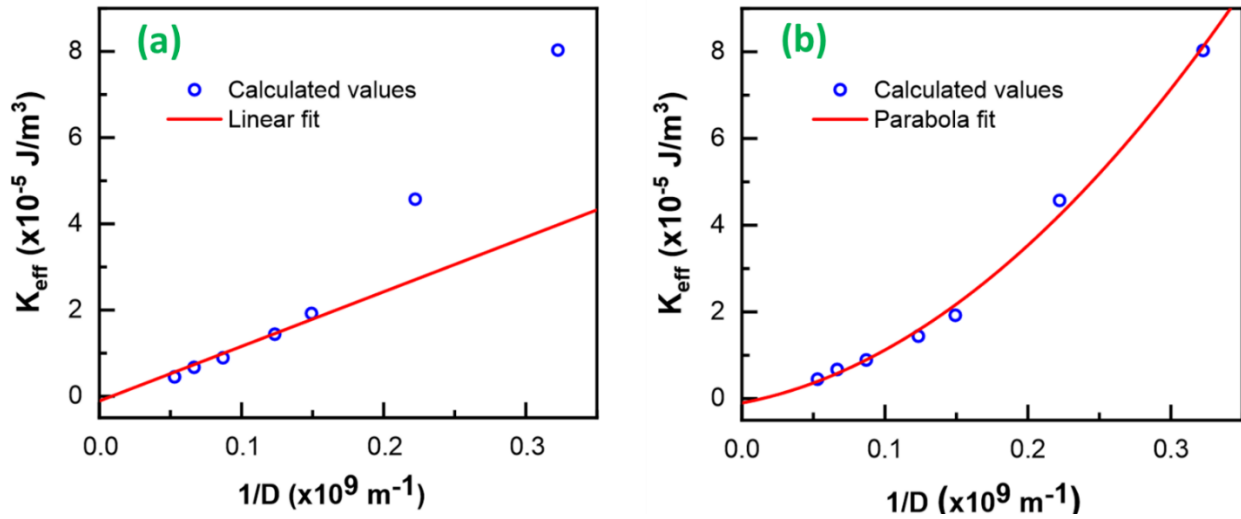


Fig. 3 fitting the K_{eff} vs. $1/D$ data using (a) Eq. (5) and (b) Eq. (6)

Table 2 The calculated K_{eff} values of the Dex-M-XX nanoparticles.

Sample Dex-M-XX	M-80	M-120	M-140	M-160	M-180	M-220	M-220
$K_{\text{eff}} (\times 10^5 \text{ J/m}^3)$	8.03	4.57	1.92	1.44	0.89	0.97	0.45

3. Conclusion

We have successfully used a series of magnetite (Fe_3O_4) nanoparticles of increasing sizes from 3.1 to 18.9 nm to investigate size-dependent changes in their magnetic properties. Our results revealed that the decrease in the saturation magnetization M_s with decreasing size can be explained by a magnetically-disordered surface layer, and fitting the experimental data the values of the magnetic dead layer thickness and M_s were estimated as $t = 6.8 \text{ \AA}$ and $M_s = 98.8 \text{ emu/g}$, respectively. We used a modified relation for calculating the contribution of the surface anisotropy K_S to the effective anisotropy K_{eff} by adding the contributions from dipolar interactions to the original model proposed by Bødker et al., obtaining a good fit for the whole range of MNPs sizes. Our analysis provides a more clear picture of the effects from the spin-disordered surface configuration on the magnetic properties in MNPs of diverse sizes. .

References

1. Issa, B., et al., *Magnetic nanoparticles: surface effects and properties related to biomedicine applications*. International journal of molecular sciences, 2013. **14**(11): p. 21266-21305.
2. Xi, S.B., et al., *Surface spin-glass, large surface anisotropy, and depression of magnetocaloric effect in $\text{La}(0.8)\text{Ca}(0.2)\text{MnO}(3)$ nanoparticles*. Journal of applied physics, 2012. **112**(12): p. 123903-123903.
3. Reyes-Ortega, F., Á.V. Delgado, and G.R. Iglesias, *Modulation of the Magnetic Hyperthermia Response Using Different Superparamagnetic Iron Oxide Nanoparticle Morphologies*. Nanomaterials, 2021. **11**(3): p. 627.
4. Soleymani, M., et al., *One-pot preparation of hyaluronic acid-coated iron oxide nanoparticles for magnetic hyperthermia therapy and targeting CD44-overexpressing cancer cells*. Carbohydrate Polymers, 2020. **237**: p. 116130.

5. Asgari, M., et al., *Design of thermosensitive polymer-coated magnetic mesoporous silica nanocomposites with a core-shell-shell structure as a magnetic/temperature dual-responsive drug delivery vehicle*. *Polymers for Advanced Technologies*.
6. Oltolina, F., et al., *Biomimetic Magnetite Nanoparticles as Targeted Drug Nanocarriers and Mediators of Hyperthermia in an Experimental Cancer Model*. *Cancers*, 2020. **12**(9): p. 2564.
7. Soleymani, M., et al., *Effects of multiple injections on the efficacy and cytotoxicity of folate-targeted magnetite nanoparticles as theranostic agents for MRI detection and magnetic hyperthermia therapy of tumor cells*. *Scientific Reports*, 2020. **10**(1): p. 1695.
8. Dong, P., et al., *Controllable synthesis of exceptionally small-sized superparamagnetic magnetite nanoparticles for ultrasensitive MR imaging and angiography*. *Journal of Materials Chemistry B*, 2021. **9**(4): p. 958-968.
9. Cole, A.J., et al., *Polyethylene glycol modified, cross-linked starch-coated iron oxide nanoparticles for enhanced magnetic tumor targeting*. *Biomaterials*, 2011. **32**(8): p. 2183-2193.
10. Shaterabadi, Z., G. Nabiyouni, and M. Soleymani, *Physics responsible for heating efficiency and self-controlled temperature rise of magnetic nanoparticles in magnetic hyperthermia therapy*. *Progress in Biophysics and Molecular Biology*, 2017.
11. Fonseca, F., et al., *Superparamagnetism and magnetic properties of Ni nanoparticles embedded in SiO₂*. *Physical review B*, 2002. **66**(10): p. 104406.
12. Espinola-Portilla, F., et al., *Superparamagnetic iron oxide nanoparticles functionalized with a binary alkoxy silane array and poly (4-vinylpyridine) for magnetic targeting and pH-responsive release of doxorubicin*. *New Journal of Chemistry*, 2021. **45**(7): p. 3600-3609.
13. Köhler, T., et al., *Mechanism of magnetization reduction in iron oxide nanoparticles*. *Nanoscale*, 2021. **13**(14): p. 6965-6976.
14. Jr., E.L., et al., *Spin disorder and magnetic anisotropy in Fe₃O₄ nanoparticles*. *Journal of Applied Physics*, 2006. **99**(8): p. 083908.
15. Kale, A., S. Gubbala, and R.D.K. Misra, *Magnetic behavior of nanocrystalline nickel ferrite synthesized by the reverse micelle technique*. *Journal of Magnetism and Magnetic Materials*, 2004. **277**(3): p. 350-358.
16. Asiri, S., et al., *The temperature effect on magnetic properties of NiFe₂O₄ nanoparticles*. *Journal of Inorganic and Organometallic Polymers and Materials*, 2018. **28**(4): p. 1587-1597.
17. Kandasamy, G. and D. Maity, *Recent advances in superparamagnetic iron oxide nanoparticles (SPIONs) for in vitro and in vivo cancer nanotheranostics*. *International Journal of Pharmaceutics*, 2015.
18. Ramimoghadam, D., S. Bagheri, and S.B.A. Hamid, *Progress in electrochemical synthesis of magnetic iron oxide nanoparticles*. *Journal of Magnetism and Magnetic Materials*, 2014. **368**: p. 207-229.
19. Curiale, J., et al., *Magnetic dead layer in ferromagnetic manganite nanoparticles*. *Applied Physics Letters*, 2009. **95**(4): p. 043106.
20. Muroi, M., et al., *Magnetic properties of ultrafine MnFe₂O₄ powders prepared by mechanochemical processing*. *Physical Review B*, 2001. **63**(18): p. 184414.
21. Nathani, H., S. Gubbala, and R. Misra, *Magnetic behavior of nanocrystalline nickel ferrite: Part I. The effect of surface roughness*. *Materials Science and Engineering: B*, 2005. **121**(1): p. 126-136.

22. Nathani, H., S. Gubbala, and R. Misra, *Magnetic behavior of nickel ferrite–polyethylene nanocomposites synthesized by mechanical milling process*. Materials Science and Engineering: B, 2004. **111**(2): p. 95-100.
23. Kodama, R.H. and A.E. Berkowitz, *Atomic-scale magnetic modeling of oxide nanoparticles*. Physical Review B, 1999. **59**(9): p. 6321.
24. Iglesias, Ó. and A. Labarta, *Finite-size and surface effects in maghemite nanoparticles: Monte Carlo simulations*. Physical Review B, 2001. **63**(18): p. 184416.
25. Kim, B.H., et al., *Large-Scale Synthesis of Uniform and Extremely Small-Sized Iron Oxide Nanoparticles for High-Resolution T1 Magnetic Resonance Imaging Contrast Agents*. Journal of the American Chemical Society, 2011. **133**(32): p. 12624-12631.
26. Gonzalez-Fernandez, M., et al., *Magnetic nanoparticles for power absorption: Optimizing size, shape and magnetic properties*. Journal of Solid State Chemistry, 2009. **182**(10): p. 2779-2784.
27. Lv, Y., et al., *Size dependent magnetic hyperthermia of octahedral Fe₃O₄ nanoparticles*. RSC Advances, 2015. **5**(94): p. 76764-76771.
28. Ma, M., et al., *Size dependence of specific power absorption of Fe₃O₄ particles in AC magnetic field*. Journal of Magnetism and Magnetic Materials, 2004. **268**(1-2): p. 33-39.
29. Tong, S., et al., *Size-Dependent Heating of Magnetic Iron Oxide Nanoparticles*. ACS Nano, 2017. **11**(7): p. 6808-6816.
30. Wang, X., H. Gu, and Z. Yang, *The heating effect of magnetic fluids in an alternating magnetic field*. Journal of Magnetism and Magnetic Materials, 2005. **293**(1): p. 334-340.
31. Yamamoto, Y., et al., *Size dependence study on magnetic heating properties of superparamagnetic iron oxide nanoparticles suspension*. Journal of Applied Physics, 2014. **116**(12): p. 123906.
32. Shirsath, S.E., et al., *Effect of sintering temperature and the particle size on the structural and magnetic properties of nanocrystalline Li_{0.5}Fe_{2.5}O₄*. Journal of magnetism and magnetic materials, 2011. **323**(23): p. 3104-3108.
33. Kim, T. and M. Shima, *Reduced magnetization in magnetic oxide nanoparticles*. Journal of applied physics, 2007. **101**(9): p. 09M516.
34. Caruntu, D., G. Caruntu, and C.J. O'Connor, *Magnetic properties of variable-sized Fe₃O₄ nanoparticles synthesized from non-aqueous homogeneous solutions of polyols*. Journal of physics D: Applied physics, 2007. **40**(19): p. 5801.
35. Shaterabadi, Z., G. Nabiyouni, and M. Soleymani, *Correlation between effects of the particle size and magnetic field strength on the magnetic hyperthermia efficiency of dextran-coated magnetite nanoparticles*. Materials Science and Engineering: C, 2020. **117**: p. 111274.
36. Wu, W., Q. He, and C. Jiang, *Magnetic iron oxide nanoparticles: synthesis and surface functionalization strategies*. Nanoscale research letters, 2008. **3**(11): p. 397-415.
37. Lu, W., et al., *Facile synthesis and characterization of polyethylenimine-coated Fe(3)O(4) superparamagnetic nanoparticles for cancer cell separation*. Mol Med Rep, 2014. **9**(3): p. 1080-4.
38. Liu, F., et al., *Novel nanopyramid arrays of magnetite*. Advanced materials, 2005. **17**(15): p. 1893-1897.
39. Shaterabadi, Z., G. Nabiyouni, and M. Soleymani, *High impact of in situ dextran coating on biocompatibility, stability and magnetic properties of iron oxide nanoparticles*. Materials Science and Engineering: C, 2017. **75**: p. 947-956.
40. Shaterabadi, Z., G. Nabiyouni, and M. Soleymani, *Optimal size for heating efficiency of superparamagnetic dextran-coated magnetite nanoparticles for application in magnetic*

- fluid hyperthermia*. Physica C: Superconductivity and its Applications, 2018. **549**: p. 84-87.
41. Kotoulas, A., et al., *The Effect of Polyol Composition on the Structural and Magnetic Properties of Magnetite Nanoparticles for Magnetic Particle Hyperthermia*. Materials, 2019. **12**(17): p. 2663.
 42. Mürbe, J., A. Rechtenbach, and J. Töpfer, *Synthesis and physical characterization of magnetite nanoparticles for biomedical applications*. Materials Chemistry and Physics, 2008. **110**(2): p. 426-433.
 43. Gnanaprakash, G., et al., *Effect of Digestion Time and Alkali Addition Rate on Physical Properties of Magnetite Nanoparticles*. The Journal of Physical Chemistry B, 2007. **111**(28): p. 7978-7986.
 44. Cullity, B.D. and C.D. Graham, *Introduction to magnetic materials*. 2011: John Wiley & Sons.
 45. Chaki, S., et al., *Magnetite Fe₃O₄ nanoparticles synthesis by wet chemical reduction and their characterization*. Advances in Natural Sciences: Nanoscience and Nanotechnology, 2015. **6**(3): p. 035009.
 46. Chen, J., et al., *Size-dependent magnetic properties of MnFe₂O₄ fine particles synthesized by coprecipitation*. Physical review B, 1996. **54**(13): p. 9288.
 47. Zheng, M., et al., *Magnetic properties of nanosized MnFe₂O₄ particles*. Journal of Magnetism and Magnetic Materials, 1998. **183**(1): p. 152-156.
 48. Liu, C. and Z.J. Zhang, *Size-Dependent Superparamagnetic Properties of Mn Spinel Ferrite Nanoparticles Synthesized from Reverse Micelles*. Chemistry of Materials, 2001. **13**(6): p. 2092-2096.
 49. Grigorova, M., et al., *Magnetic properties and Mössbauer spectra of nanosized CoFe₂O₄ powders*. Journal of magnetism and magnetic materials, 1998. **183**(1-2): p. 163-172.
 50. Jiang, J., G. Goya, and H. Rechenberg, *Magnetic properties of nanostructured CuFe₂O₄*. Journal of Physics: Condensed Matter, 1999. **11**(20): p. 4063.
 51. Brown Jr, W.F., *Theory of the approach to magnetic saturation*. Physical Review, 1940. **58**(8): p. 736.
 52. Martinez-Boubeta, C., et al., *Learning from nature to improve the heat generation of iron-oxide nanoparticles for magnetic hyperthermia applications*. Scientific reports, 2013. **3**: p. 1652.
 53. Jin, Z.-Q., et al., *Effective magnetic anisotropy of nanocrystalline Nd-Fe-Ti-N hard magnetic alloys*. The European Physical Journal B-Condensed Matter and Complex Systems, 1998. **3**(1): p. 41-44.
 54. Andreev, S., et al., *Law of approach to saturation in highly anisotropic ferromagnets Application to Nd-Fe-B melt-spun ribbons*. Journal of alloys and compounds, 1997. **260**(1-2): p. 196-200.
 55. Sarkar, D. and M. Mandal, *Static and dynamic magnetic characterization of DNA-templated chain-like magnetite nanoparticles*. The Journal of Physical Chemistry C, 2012. **116**(5): p. 3227-3234.
 56. Engelmann, U.M., et al., *Heating efficiency of magnetic nanoparticles decreases with gradual immobilization in hydrogels*. Journal of Magnetism and Magnetic Materials, 2019. **471**: p. 486-494.
 57. Carrey, J., B. Mehdaoui, and M. Respaud, *Simple models for dynamic hysteresis loop calculations of magnetic single-domain nanoparticles: Application to magnetic hyperthermia optimization*. Journal of Applied Physics, 2011. **109**(8): p. 083921.

58. Dennis, C.L. and R. Ivkov, *Physics of heat generation using magnetic nanoparticles for hyperthermia*. Int J Hyperthermia, 2013. **29**(8): p. 715-29.
59. Goya, G.F. and M. Morales. *Field dependence of blocking temperature in magnetite nanoparticles*. in *Journal of Metastable and Nanocrystalline Materials*. 2004. Trans Tech Publ.
60. Kechrakos, D. and K. Trohidou, *Competition between dipolar and exchange interparticle interactions in magnetic nanoparticle films*. Journal of magnetism and magnetic materials, 2003. **262**(1): p. 107-110.
61. Pauly, M., et al., *Size dependent dipolar interactions in iron oxide nanoparticle monolayer and multilayer Langmuir–Blodgett films*. Journal of Materials Chemistry, 2012. **22**(13): p. 6343-6350.
62. Bødker, F., S. Mørup, and S. Linderøth, *Surface effects in metallic iron nanoparticles*. Physical Review Letters, 1994. **72**(2): p. 282-285.
63. Bartolomé, J., et al., *Magnetic polarization of noble metals by Co nanoparticles in M-capped granular multilayers (M= Cu, Ag, and Au): An x-ray magnetic circular dichroism study*. Physical Review B, 2008. **77**(18): p. 184420.
64. Luis, F., et al., *Enhancement of the magnetic anisotropy of nanometer-sized Co clusters: Influence of the surface and of interparticle interactions*. Physical Review B, 2002. **65**(9): p. 094409.
65. Yu, D., et al., *Crystal phase, morphology evolution and luminescence properties of Eu³⁺-doped BiPO₄ phosphor prepared using the hydrothermal method*. Luminescence, 2021. **36**(5): p. 1143-1150.
66. Wang, W., *Facile hydrothermal synthesis of ZnCo₂O₄ nanostructures: controlled morphology and magnetic properties*. Journal of Materials Science: Materials in Electronics, 2021: p. 1-7.
67. Chen, D., X. Jiao, and G. Cheng, *Hydrothermal synthesis of zinc oxide powders with different morphologies*. Solid State Communications, 1999. **113**(6): p. 363-366.
68. Gorenstein, M.I. and W. Greiner, *Linear chains of dipoles and magnetic susceptibility*. Modern Physics Letters B, 2014. **28**(05): p. 1450039.
69. Anand, M., *Hysteresis in a linear chain of magnetic nanoparticles*. Journal of Applied Physics, 2020. **128**(2): p. 023903.
70. Butter, K., et al., *Direct observation of dipolar chains in iron ferrofluids by cryogenic electron microscopy*. Nature materials, 2003. **2**(2): p. 88-91.
71. Morales, I., et al., *High Frequency Hysteresis Losses on γ -Fe₂O₃ and Fe₃O₄: Susceptibility as a Magnetic Stamp for Chain Formation*. Nanomaterials, 2018. **8**(12): p. 970.
72. Myrovali, E., et al., *Arrangement at the nanoscale: Effect on magnetic particle hyperthermia*. Scientific Reports, 2016. **6**(1): p. 37934.
73. Martinez-Boubeta, C., et al., *Learning from Nature to Improve the Heat Generation of Iron-Oxide Nanoparticles for Magnetic Hyperthermia Applications*. Scientific Reports, 2013. **3**(1): p. 1652.